remote sensing

MDPI

Article

Multispectral vs. RGB UAV Imagery for Detecting Mistletoe (*Viscum album*) in Scots Pine Forests: Identifying the Most Informative Vegetation Indices

Jakub Miszczyszyn [1], Piotr Wężyk [1,2], Luiza Tymińska-Czabańska [1], Jarosław Socha [1] and Marta Szostak [1,*]

[1] Department of Forest Resources Management, Faculty of Forestry, University of Agriculture in Krakow, al. Mickiewicza 21, 31-120 Kraków, Poland; jakub.miszczyszyn@urk.edu.pl (J.M.)
[2] ProGea SKY Ltd., 31-223 Kraków, Poland
* Correspondence: marta.szostak@urk.edu.pl

Highlights

What are the main findings?

- UAV-based multispectral imagery classification achieved accuracy of 0.82 and Kappa of 0.74 for mistletoe detection.
- Approximately 58.6% of Scots pine trees in the 22.5 ha study area were infected with mistletoe, with a total biogroup area of 489 m^2.
- UAV cameras equipped with a near-infrared (NIR) channel provide substantially better mistletoe discrimination than RGB-only systems, confirming NIR as an essential band for operational forest-health monitoring.

What are the implications of the main findings?

- Green-sensitive and NIR-based vegetation indices provide effective spectral features for automated mistletoe detection, enabling forest health monitoring.
- The proposed methodology offers a non-invasive, repeatable approach for quantifying mistletoe infestation at the individual tree level, supporting evidence-based forest management decisions.

Abstract

The aim of this study was to examine the potential of multispectral imaging derived from unmanned aerial vehicles (UAVs) for detecting the spread of mistletoe (*Viscum album* ssp. *austriacum* L.) in Scots pine stands and to assess the information potential of selected vegetation indices in mistletoe detection. UAV campaigns were performed in the Niepołomice Primeval Forest (Niepołomice Forest District, Regional Directorate of the Polish State Forests National Holding, Kraków, Poland). A fixed-wing UAV Trinity F90+ (Quantum Systems GmbH) equipped with a five-band multispectral MicaSense RedEdge-M camera and an RGB Sony UMC-R10C camera was employed. The number of trees infected by mistletoe, as well as the quantity and area of mistletoe biogroups, were derived based on the classification of true multispectral orthophotos using a support vector machine (SVM) classifier. The spectral information potential assessment identified NIR (B5) as the most important single spectral source of information, while the greatest information potential among vegetation indices was found in NormG, CIG, and GRVI. The mistletoe classification of the 22.5-ha compartment revealed 1735 mistletoe biogroups covering a total area of 489 m^2, with 58.6% of the 2917 detected tree crowns identified as infected (Kappa = 0.74). The results confirm that UAV-based multispectral data, particularly when

Check for updates

Academic Editor: Liming Zhou

Received: 12 March 2026
Revised: 12 May 2026
Accepted: 14 May 2026
Published: 16 May 2026

Copyright: © 2026 by the authors. Licensee MDPI, Basel, Switzerland. This article is an open access article distributed under the terms and conditions of the Creative Commons Attribution (CC BY) license.

combined with green-sensitive vegetation indices, enable effective differentiation of mistletoe from host tree crowns. The integration of the near-infrared (NIR) band further enhanced classification performance. This study evaluates UAV-based multispectral and RGB imagery for detecting common mistletoe (*Viscum album* ssp. austriacum) in Scots pine stands. The information potential of 22 vegetation indices was assessed to identify the most effective spectral features for mistletoe classification.

Keywords: mistletoe; *Viscum album*; UAV; multispectral imagery; vegetation indices; SVM classification; Scots pine; forest health monitoring; remote sensing; NIR

1. Introduction

Climate change-induced weather extremes witnessed in recent decades have affected the health of forest stands. These extremes may be one cause of forest degradation and increasingly observed widespread tree mortality [1]. The widespread forest decline poses challenges to foresters who frequently struggle to track forest decline across wide areas. The intensive development of remote sensing techniques has led to new possibilities for effectively monitoring forest health conditions [2]. High-resolution multispectral photographs collected by unmanned aerial vehicles (UAVs) are a relatively new tool for detecting and modelling disturbances in forest areas. UAV-based data thereby contribute to a better understanding of forest ecosystem functioning and the assessment of ecosystem services under a changing climate [3].

As a result of climate change, the intensive expansion of mistletoe in the forests of Poland and Europe has been observed in recent years. Accelerated tree mortality and severe damage caused by common mistletoe (*Viscum album* ssp. *austriacum*) in Scots pine stands has become an increasing concern in several countries across Europe [4]. Stress induced by climate change-related extreme weather events enables pathogens like mistletoe to more efficiently overcome the defence mechanisms of trees. In recent decades, many areas in Poland have experienced increases in average air temperature and decreases in groundwater levels. The resulting soil drought has notably contributed to the weakening of forest stands [5]. As a semi-parasite, mistletoe drains water and mineral nutrients from the host tree, increasing its water deficit during periods of drought. The intensive gas exchange of the mistletoe, which continues despite the closure of stomata of the host tree, further weakens it [6]. The problem of common mistletoe (*Viscum album* L.) infestations is of great economic importance. Scots pine (*Pinus sylvestris* L.) is the most important forest-forming species in Poland, occupying 58.7% of the forest area in all forms of ownership [7]. Changes in climate, particularly increases in temperature, may lead to the expansion of mistletoe into regions of Europe where it was previously absent [8]. Trees colonized by mistletoe are characterized by lower harvesting abundance, lower seed mass with poorer germination capacity, and poorer quality of seedlings [9]. Research conducted in the Bolewice Forest District confirmed the negative effect of spreading mistletoe on infected versus infection-free trees [10]. The radial growth of a tree affected by mistletoe can be reduced by up to 65% [3,11]. Pilichowski et al. (2018) documented a radial growth reduction of up to 37% in Poland [12]. Inventorying mistletoe infestation in pine stands is therefore crucial for making appropriate forest management decisions [13].

European forest management currently lacks developed standards and methods for automatic yet rapid detection of mistletoe. The assessment of mistletoe occurrence is usually performed by traditional time-consuming techniques based on ground observations [14]. Mistletoe infects shoots and branches located in the upper parts of the tree crown.

The number of trees affected by mistletoe infections is therefore often underestimated in ground-based inventories [15]. The colour similarity of mistletoe to deciduous tree crowns and the dense opaque canopy further complicate detection. Remote sensing techniques, allowing for a top-view of the canopy, represent a suitable approach for collecting information on mistletoe infection rapidly and precisely. Several studies focusing on mistletoe detection have been presented, including work on eucalyptus trees in Australia [16] and comparisons of UAV and satellite imagery [17]. While most UAV systems operate with high-resolution RGB cameras, multispectral cameras collecting information in the Red Edge, near-infrared (NIR), and thermal infrared (TIR) bands may enable better distinction of tree health states [18]. Vegetation indices (VIs), which are mathematical combinations of two or more spectral bands, are widely applied in remote sensing. However, their use for automatic mistletoe detection has not yet been examined in detail.

The aim of this study was to investigate the potential of UAV-derived multispectral imaging for inventorying mistletoe (*Viscum album* ssp. *austriacum* L.) in Scots pine stands. An additional objective was to determine which vegetation indices have the greatest informative potential for mistletoe detection.

2. Materials and Methods

2.1. Study Area

The study area was located in the Niepołomice Primeval Forest, within the territory of the Niepołomice Forest District, forest compartment 83 in Wola Batorska (Figure 1). The area of compartment 83 is 22.5 ha. The dominant species in the compartment is Scots pine.

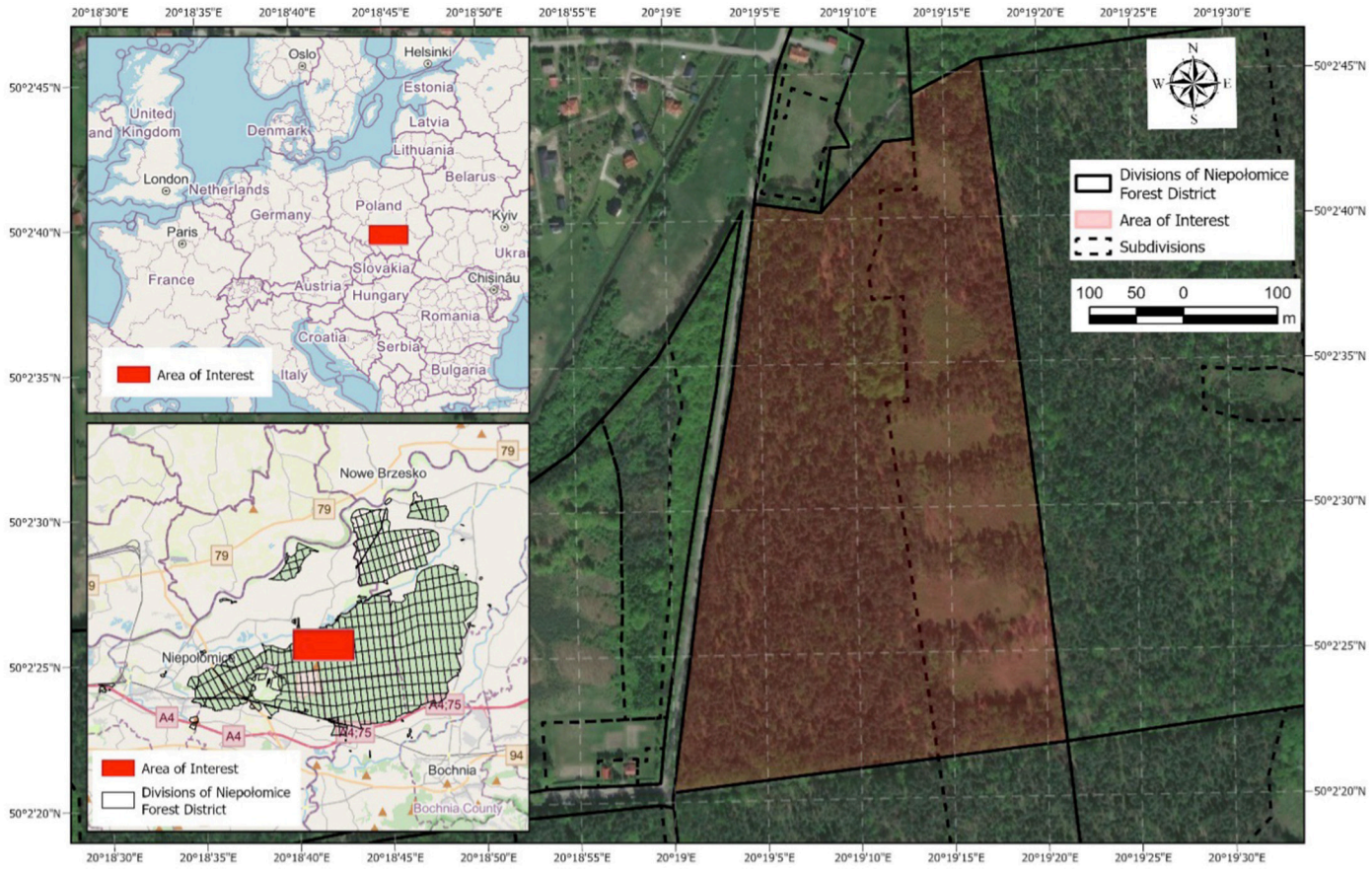


Figure 1. Location of the study area in the Niepołomice Primeval Forest, southern Poland.

2.2. Data Acquisition

RGB and multispectral (MS) images were acquired using specified camera payloads and a UAV platform. Airborne laser scanning (ALS) LiDAR 3D point clouds in LAS format were acquired in 2019 (density 4 pts/m^2; Standard I) and obtained from the GUGiK repository. GIS vector layers of the forest digital map were available from the Forest Data Bank repository (www.bdl.lasy.gov.pl/portal/; accessed on 21 January 2022.) containing the polygons of forest subcompartments and compartments with biometric taxation parameters.

2.2.1. UAV Platform and Equipment

The UAV platform employed was the fixed-wing VTOL (Vertical Take-Off and Landing) Trinity F90+ (Quantum Systems GmbH, Gilching, Germany). The platform features a dedicated payload section for interchangeable cameras. The digital cameras used were: Sony UMC-R10C (Sony Corporation, Tokyo, Japan; 20.1 Mpx resolution, APS-C sensor) and MicaSense RedEdge-M (MicaSense Inc., Seattle, WA, USA; Table 1). The multispectral camera records five bands: Blue (centre wavelength: 475 nm, bandwidth: 20 nm), Green (560 nm, 20 nm), Red (668 nm, 10 nm), Red Edge (717 nm, 10 nm), and Near-Infrared—NIR (840 nm, 40 nm).

Table 1. Spectral bands of MicaSense RedEdge-M multispectral camera with corresponding Sentinel-2 bands.

Abbreviation	Band	Central Wavelength [nm]	Bandwidth [nm]	Sentinel-2 Band
B1	Blue	~475	~20	Band 2 (~490 nm)
B2	Green	~560	~20	Band 3 (~560 nm)
B3	Red	~668	~10	Band 4 (~665 nm)
B4	Red Edge	~717	~10	Band 5 (~705 nm)
B5	NIR (IR)	~840	~40	Band 8 (~842 nm)

2.2.2. Software

The methodology required the use of dedicated software for UAV flight mission planning, photograph processing, and spatial GIS analysis. QBase 3D v2.2.11 (Quantum Systems GmbH), licensed from Progea SKY Ltd. (Kraków, Poland), was employed for designing the photogrammetric mission, monitoring its progress, and assigning GeoTags to the UAV photographs. Agisoft Metashape Professional ver. 1.5.5 (Agisoft LLC, St. Petersburg, Russia) was utilized to process the acquired photographs and generate 3D point clouds (dense matching), elevation models, and true orthophotos. ArcGIS Pro ver. 2.9.1 (Esri, Redlands, CA, USA) was used for spatial analysis, supervised classification, and visualization of results. The R programming language was used for automated generation of vegetation index rasters and normalization of ALS point clouds, as well as for generating the canopy height model (CHM) using the "lidR" [19] and "raster" [20] packages.

2.2.3. Photogrammetric Mission Planning

The Trinity F90+ UAV carried out the designed mission in automatic mode using QBase 3D software. The operator assessed the terrain and potential sources of radio wave interference. The selection of take-off, landing, and emergency landing sites followed the requirements of the Visual Line of Sight (VLOS) flight scenario. The following parameters were assumed: flight altitude of 100 m above ground level (AGL), cross-country flights with 67% longitudinal coverage and 75% transverse coverage, a local base station for Global

Navigation Satellite System (GNSS) Post-Processing Kinematic (PPK) processing, and the acquisition of RGB and multispectral images with Ground Sampling Distance (GSD) of 2.6 cm and 7 cm, respectively.

2.2.4. UAV Data Processing

After image transfer, geotagging was performed using QBase 3D, assigning coordinates from the flight log to each image's projection centre. The orthoimage generation was carried out using Agisoft Metashape Professional v1.5.5. Internal orientation parameters, including the camera constant and distortion coefficients, were adjusted through self-calibration. External orientation parameters were calculated using aerial triangulation with bundle block adjustment. Dense point clouds were generated using depth maps derived from overlapping stereo pairs. Manual corrections removed artefacts, and isolated points were filtered out. True orthoimages were created using original images projected onto the digital surface model (DSM). RGB images achieved a GSD of 2.6 cm, while MS images had a GSD of 7 cm.

The MicaSense RedEdge-M multispectral imagery was radiometrically calibrated through the manufacturer's two-stage workflow. First, images of the MicaSense Calibrated Reflectance Panel (CRP) were acquired immediately before take-off and immediately after landing under stable illumination; per-band CRP reflectance values (provided by the manufacturer) were used to derive the digital number to surface reflectance conversion coefficients for each flight. Second, the MicaSense Downwelling Light Sensor 2 (DLS2) (MicaSense, Seattle, WA, USA), mounted on the upper fuselage of the Trinity F90+ UAV, continuously recorded incident solar irradiance per band during the flight; these per-image irradiance measurements were applied in Agisoft Metashape Professional v1.5.5 during orthomosaic generation to correct for between-image illumination variation arising from changes in solar geometry over the course of the mission. The UAV campaign was conducted in July 2020 under cloudless sky and calm wind conditions, within the local solar window of approximately 10:30–15:00 CEST, corresponding to solar elevation angles between 50° and 61° (peak ~61° around local solar noon).

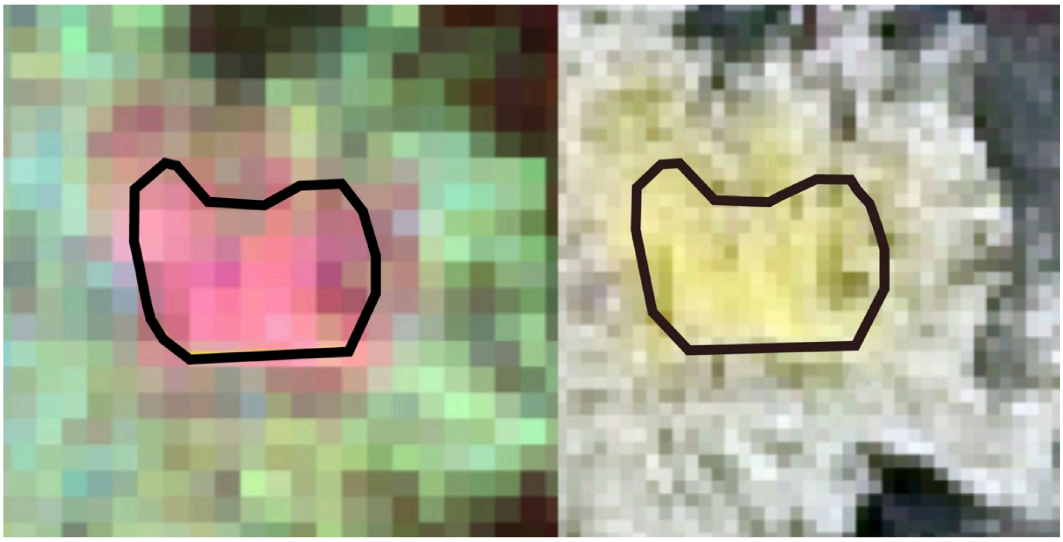
2.3. Preprocessing and Vegetation Index Calculation

The "rsi" package was utilized, providing access to a database of spectral indices (Table 2), including formulas, domains of use, and links to relevant publications [21]. The indices were categorised according to the bands required for their calculation: indices using only visible bands (Blue, Green, Red; labelled RGB' in Table 2) and indices requiring also the Red Edge and/or NIR bands (labelled 'MS'). All indices were computed from the MicaSense RedEdge-M orthomosaic at 7 cm GSD; the RGB' label denotes the band requirement of the index formula, not the sensor from which it was derived.

Segment-level statistics were computed for the training polygons using an R script. The 190 training polygons (five classes, described in Section 2.5) were vectorised manually at locations distributed across the entire 22.5-ha compartment, with operator verification against both the multispectral (NIR-Red-Green false-colour composite) and the RGB orthomosaics (Figure 2). Separately, a 1-ha test site within the compartment was vectorised at full polygon-level detail (85 mistletoe biogroups) and used as the reference dataset for the segmentation parameter selection described in Section 3.1.

Table 2. Summary of vegetation indices used in this study [21].

Index Full Name	Category	Formula	Abbrev.	Ref.
Green Leaf Index	RGB	$(2.0 \times G - R - B)/(2.0 \times G + R + B)$	GLI	[22]
Normalized Green Red Difference Index	RGB	$(G - R)/(G + R)$	NGRDI	[23]
Triangular Greenness Index	RGB	$-0.5 \times (190 \times (R - G) - 120 \times (R - B))$	TGI	[24]
Visible Atmospherically Resistant Index	RGB	$(G - R)/(G + R - B)$	VARI	[25]
Vegetation Index Green	RGB	$(G - R)/(G + R)$	VIG	[25]
Anthocyanin Reflectance Index	MS	$(1/G) - (1/RE1)$	ARI	[26]
Blue NDVI	MS	$(N - B)/(N + B)$	BNDVI	[27]
Chlorophyll Index Green	MS	$(N/G) - 1.0$	CIG	[28]
Chlorophyll Index Red Edge	MS	$(N/RE1) - 1$	CIRE	[28]
Chlorophyll Vegetation Index	MS	$(N \times R)/(G^2)$	CVI	[29]
Difference Vegetation Index	MS	$N - R$	DVI	[30]
Green Atmospherically Resistant VI	MS	$(N - (G - (B - R)))/(N - (G + (B - R)))$	GARI	[31]
Green NDVI	MS	$(N - G)/(N + G)$	GNDVI	[31]
Green Optimized Soil Adjusted VI	MS	$(N - G)/(N + G + 0.16)$	GOSAVI	[32]
Green Ratio Vegetation Index	MS	N/G	GRVI	[32]
Normalized Difference Vegetation Index	MS	$(N - R)/(N + R)$	NDVI	[33]
Normalized Green	MS	$G/(N + G + R)$	NormG	[34]
Normalized NIR	MS	$N/(N + G + R)$	NormNIR	[34]
Normalized Red	MS	$R/(N + G + R)$	NormR	[34]
Optimized Soil-Adjusted VI	MS	$(N - R)/(N + R + 0.16)$	OSAVI	[35]
Simple Ratio	MS	N/R	SR	[36]
Transformed Vegetation Index	MS	$(((N - R)/(N + R)) + 0.5)^{0.5}$	TVI	[33]



(**a**) (**b**)

Figure 2. Example of a mistletoe biogroup vectorized by an operator using multispectral (MS) and RGB orthophotos simultaneously. (**a**) Mistletoe in NIR-RED-BLUE composition; (**b**) RED-GREEN-BLUE composition.

2.4. Tree Segmentation and ALS Data Processing

Airborne laser scanning data acquired in 2019 (GUGiK repository; point density 4 pts/m^2; Standard I) were processed in R v4.3.1 using the lidR package [37] following a standard area-based workflow. Ground points were identified using the Cloth Simulation Filter (CSF) and the point cloud was height-normalized against the resulting Digital Terrain Model. A Canopy Height Model (CHM) was generated at 0.5-m resolution using the pit-free algorithm (rasterize_canopy with pitfree() algorithm, subcircle radius 0.15 m). Individual tree tops were detected using local maxima filtering (locate_trees with lmf() algorithm, fixed window size 5 m), and crown polygons were delineated using the Dalponte et al. (2016) region-growing algorithm (segment_trees with dalponte2016(), threshold seed 0.45, threshold crown 0.55, maximum crown radius 10 m).

Mistletoe biogroups (classified polygons from the MS orthomosaic, Section 2.5) were associated with individual tree crowns through spatial intersection: a biogroup was assigned to a crown polygon if its centroid fell within that crown. Trees with one or more associated biogroups were classified as infected.

For the spectral signature analysis used in the information potential assessment (Sections 3.4 and 3.5), ALS-delineated crown polygons were further stratified into three categories: (i) non-infested crowns—crown polygons that did not intersect any mistletoe polygon from the training set; (ii) infested crowns—crown polygons that intersected at least one mistletoe polygon; and (iii) mistletoe—the mistletoe polygons themselves. This three-class stratification allowed comparison of spectral signatures between host trees with and without mistletoe, as well as between host tissue and mistletoe itself.

2.5. Classification Model

The information potential of the spectral feature set and mistletoe detection was assessed on 190 training polygons manually vectorised at locations distributed across the entire 22.5-ha compartment, with visual verification against both the MS (NIR-Red-Green false-colour) and RGB orthomosaics. The five classes were: A—mistletoe (100 plots), B—coniferous canopy (20), C—deciduous canopy (20), D—dead trees (20), E—ground and undergrowth (30). The raw values of the MS mosaic bands were calculated during a zonal statistical analysis in ArcGIS Pro (Esri), whilst the vegetation index values were calculated

using the R language and the terra package as the average values of all pixels within the polygons (Figure 3).

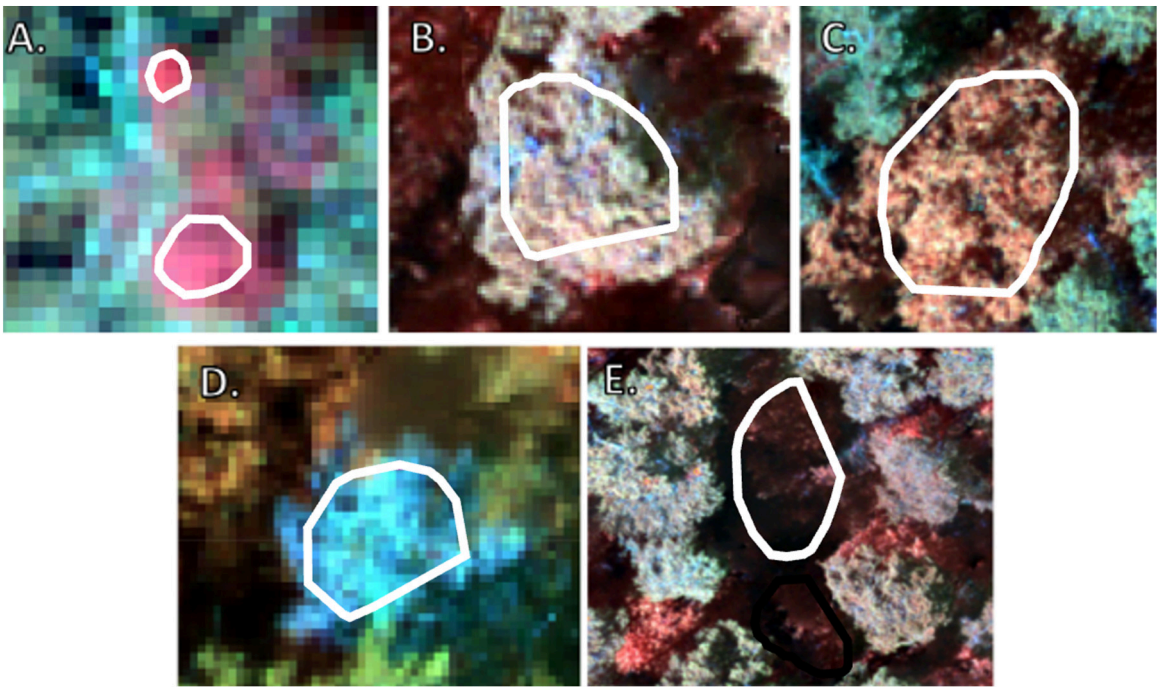


Figure 3. Training plots used in machine learning vegetation classification: (**A**) mistletoe (100 plots); (**B**) coniferous canopy (20 plots); (**C**) deciduous canopy (20 plots); (**D**) dead trees (20 plots); (**E**) ground and undergrowth (30 plots).

Image segmentation of the multispectral orthomosaic was performed in the Image Classification Wizard module in ArcGIS Pro (Esri) using the Mean Shift algorithm. Four variants of the minimum segment size were tested (1, 3, 10, and 20 pixels) to assess the impact of merging smaller segments with their best-fitting neighbours; the segmentation parameters selected on the basis of the test reported in Section 3.1 were then applied to the full 22.5-ha compartment.

The mistletoe classification was carried out in ArcGIS Pro using the Support Vector Machine (SVM) classifier from the Image Classification Wizard module. The classifier was trained on the 190 training polygons (Section 2.3) using the five raw MicaSense multispectral bands (B1–B5) as input features, and configured with default ArcGIS Pro parameters: a maximum number of samples per class set to 500, a maximum number of features per segment as automatically determined by the tool, and the default kernel and regularisation settings of the underlying scikit-learn SVM implementation used by ArcGIS Pro. No manual hyperparameter tuning was performed. The trained classifier was then applied to the segmented orthomosaic of the entire 22.5-ha compartment to produce the mistletoe biogroup map presented in Section 3.6. The accuracy of the resulting map was assessed against 477 stratified random reference points generated on the classified raster using the Create Accuracy Assessment Points tool, manually labelled by the first author through visual photo-interpretation of the MS (NIR-Red-Green false-colour composite) and the RGB orthomosaics, and processed with the Compute Confusion Matrix tool (full validation protocol in Section 2.7).

2.6. Spectral Information Potential Assessment

The spectral information potential of individual bands and vegetation indices was assessed independently of the mistletoe classification (Section 2.5), using R with the caret

and kernlab [38] packages. The 190 training polygons (Section 2.3) were used as input. For each polygon, mean values of the five raw spectral bands (B1–B5) and the 22 vegetation indices (Table 2) were extracted and used as features. The dataset was randomly partitioned into a training and a test set (50/50 stratified by class, fixed random seed = 123). An SVM classifier with a Radial Basis Function (RBF) kernel and cost parameter C = 3 was trained using the ksvm function from the kernlab package. The classifier was trained with default kernlab settings: the RBF kernel width parameter (sigma, equivalent to gamma) was estimated automatically from the training data via the kernlab::sigest function, and equal class weights were used. The 100 mistletoe training polygons against 90 polygons combined from the four background classes constitute a near-balanced design, so no class re-weighting was applied. The objective of this analysis was to characterise the relative information content of individual spectral features rather than to optimise classifier performance through hyperparameter tuning; a systematic grid search and multi-classifier benchmark are identified as future work (Section Limitations and Future Work). The overall accuracy and Kappa coefficient were computed on the test set; this was performed first on the full feature set (5 bands + 22 indices) and then repeated for selected feature subsets (raw bands only, vegetation indices only, RGB-band-derived indices only) to evaluate the information potential of different feature combinations (Section 3.2).

A leave-one-out analysis was then performed to quantify the contribution of each individual feature to the discriminative performance. The SVM was retrained iteratively, with one feature column at a time set to zero (leaving the remaining 26 features intact), and the change in accuracy and Kappa relative to the full-feature baseline was recorded. The most informative features were identified as those whose removal caused the largest decrease in classification metrics (Section 3.3).

2.7. Validation of the Mistletoe Classification

The accuracy of the mistletoe classification produced in ArcGIS Pro for the full 22.5-ha compartment (Section 2.5, results in Section 3.6) was assessed against an independent set of 477 stratified random reference points generated on the classified raster using the Create Accuracy Assessment Points tool in ArcGIS Pro. Points were stratified by classified class to ensure representation of each output class proportionally to its share of the classified area. Each point was assigned a reference class through manual photo-interpretation by the first author, performed in ArcGIS Pro on both the multispectral orthomosaic (NIR-Red-Green false-colour composite) and the RGB orthomosaic visualised side by side; the photo-interpretation was carried out without reference to the predicted class. The confusion matrix and Kappa were computed on the full set of 477 points using the Compute Confusion Matrix tool in ArcGIS Pro, and per-class user and producer accuracies were derived from the resulting matrix and reported in Section 3.6. The 477 reference points are spatially independent of the 190 training polygons used to train the classifier (Section 2.5), as they were sampled across the entire compartment from the classified output rather than drawn from the training set.

3. Results

3.1. Segmentation Parameters Testing

A 1 ha test plot of a multispectral true orthophoto (MicaSense) was subjected to four segmentation variants. The minimum number of pixels comprising a segment was set to 1, 3, 10, and 20 pixels (Figure 4). Each variant was classified based on the same training plots. The results are presented in Table 3.

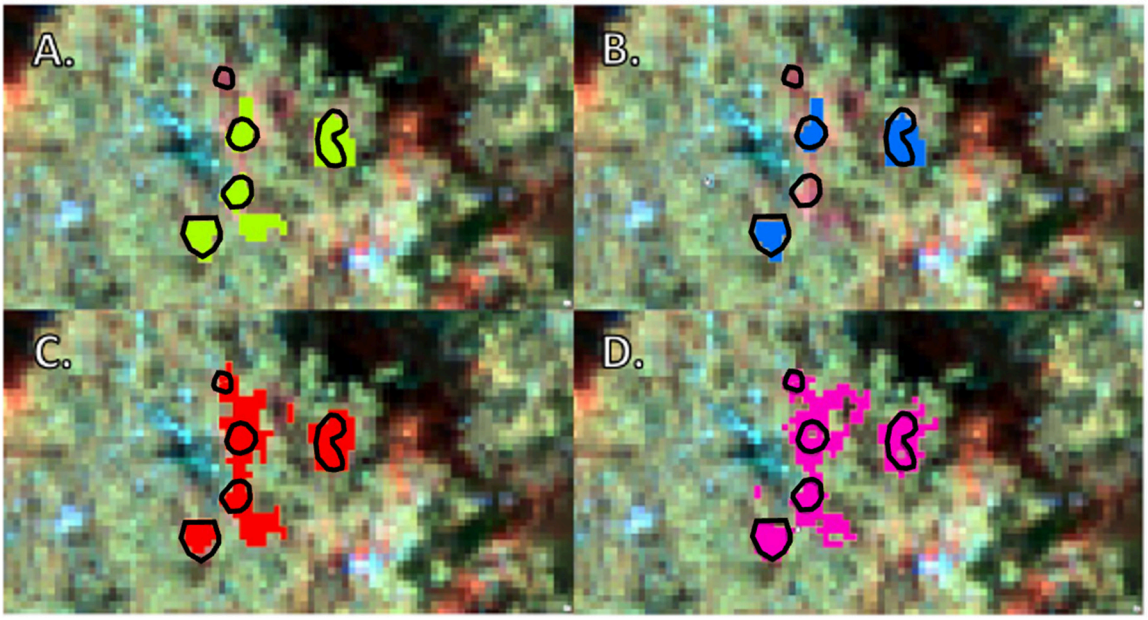


Figure 4. Classification results for different minimum segment sizes: (**A**) 10 pixels; (**B**) 20 pixels; (**C**) 3 pixels; (**D**) 1 pixel.

Table 3. Summary of classification results for different minimum segment sizes.

Min. Pixels	Detected Biogroups	Area [m^2]	Count Error [%]	Area Error [%]
20	43	22.7	−49	−29
10	77	26.8	−9	−16
3	175	40.5	+106	+27
1	744	52.2	+775	+63
Reference	85	32.0	—	—

3.2. Spectral Information Potential of Feature-Set Combinations

The highest classification performance was achieved using the combination of NIR and Red Edge bands with vegetation indices (Accuracy = 0.99, Kappa = 0.97). Using all raw spectral bands yielded an accuracy of 0.96 and Kappa of 0.92. Models based solely on vegetation indices achieved an accuracy of 0.95 and Kappa of 0.90. The use of only RGB bands led to reduced performance (Accuracy = 0.89, Kappa = 0.78). The lowest performance was observed when only NIR and Red Edge bands were used without indices (Accuracy = 0.86, Kappa = 0.73) (Table 4).

Table 4. Information potential of different feature-set combinations: accuracy and Kappa values from SVM classification on 190 training polygons (50/50 hold-out split).

Input Data	Accuracy	Kappa
NIR and Red Edge bands and VIs	0.99	0.97
Raw bands (R, G, B, NIR, Red Edge)	0.96	0.92
VIs without raw bands	0.95	0.90
RGB bands only	0.89	0.78
RGB bands and RGB-based VIs	0.88	0.76
NIR and Red Edge bands only	0.86	0.73

Per-class confusion matrices for all six feature-set combinations are presented below (Figure 5). Across all six combinations, the mistletoe class (class 1) was correctly classified in 48 or 49 of the 49 test observations. The coniferous canopy class (class 2) was correctly classified in all 5 test observations across all six combinations. The deciduous canopy class (class 3) varied from 5 correct classifications (NIR + RedEdge bands + VIs; VIs without raw bands) to 2 correct classifications (RGB bands only; RGB bands + RGB-based VIs) and 3 (Raw bands; RGB bands + RGB-based VIs; NIR + RedEdge bands only). The dead trees class (class 4) varied from 5 correct classifications (NIR + RedEdge bands + VIs; Raw bands; RGB bands only; NIR + RedEdge bands only) to 3 (VIs without raw bands) and 4 (RGB bands + RGB-based VIs). The ground and undergrowth class (class 5) was correctly classified in 9 of 10 test observations for the two highest-performing combinations (NIR + RedEdge bands + VIs; Raw bands), and varied between 4 and 8 for the remaining combinations.

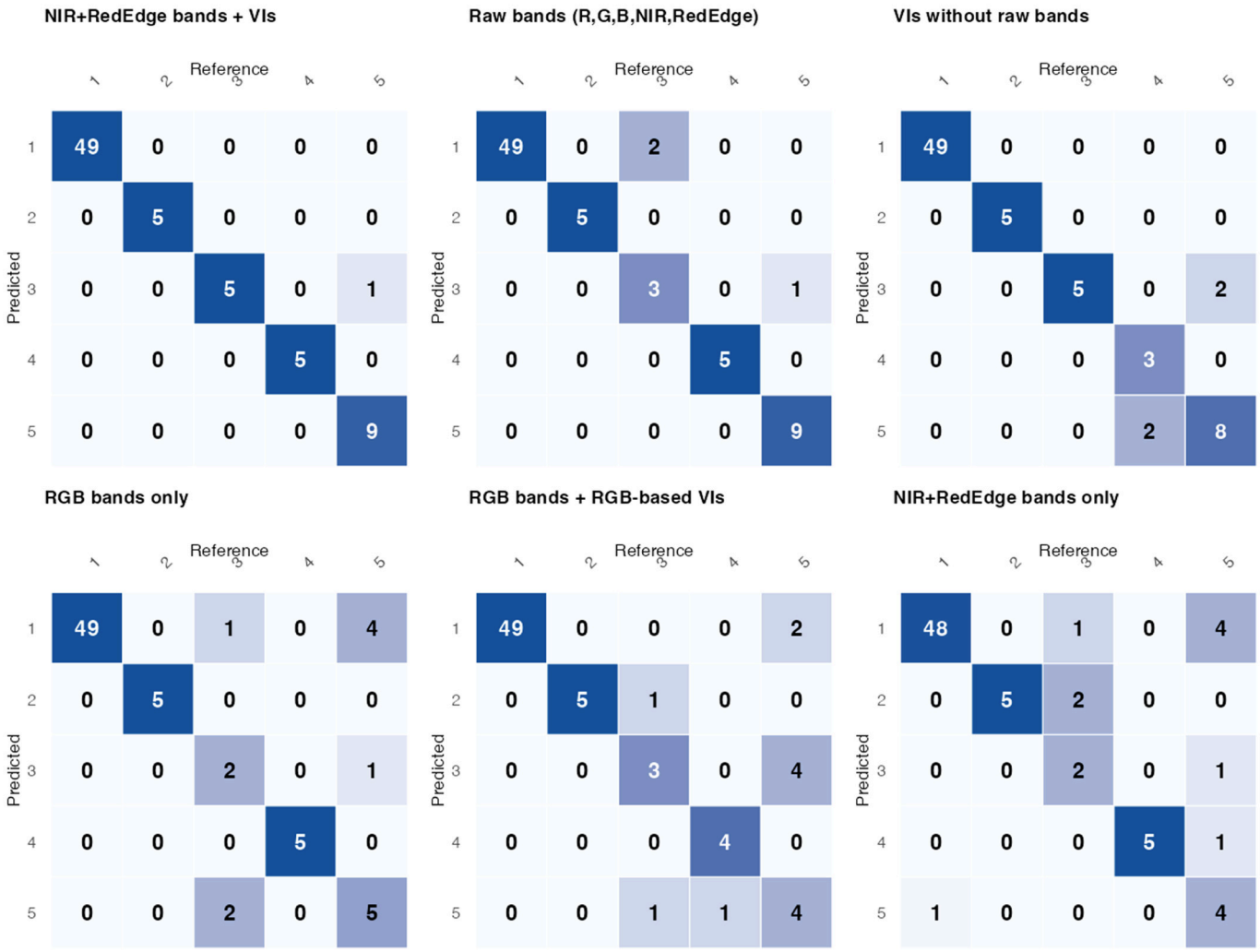


Figure 5. Per-class confusion matrices for the six feature-set combinations evaluated in the spectral information potential assessment. Each matrix corresponds to one row of Table 4 and is computed on the test subset of the 50/50 stratified hold-out split of the 190 training polygons (SVM with RBF kernel, C = 3). Row labels (Predicted) and column labels (Reference) refer to the five training classes: 1—mistletoe, 2—coniferous canopy, 3—deciduous canopy, 4—dead trees, 5—ground and undergrowth. Cell values are observation counts; cell colour intensity scales with the column-wise (per-reference-class) percentage. Overall accuracy and Cohen's Kappa coefficient for each feature-set combination are reported above each panel.

3.3. Leave-One-Out Analysis of Individual Feature Contributions

The removal of the NIR band (B5) led to the largest decrease in Kappa coefficient, exceeding 30%, and a notable drop in accuracy. Reductions in both metrics were also observed after excluding CIG, CIRE, and GNDVI. The removal of GRVI and VARI resulted in Kappa reductions of approximately 20%. Accuracy differences for these indices remained between 5–10%. TGI and Red Edge (B4) caused the smallest changes in both metrics (Figure 6).

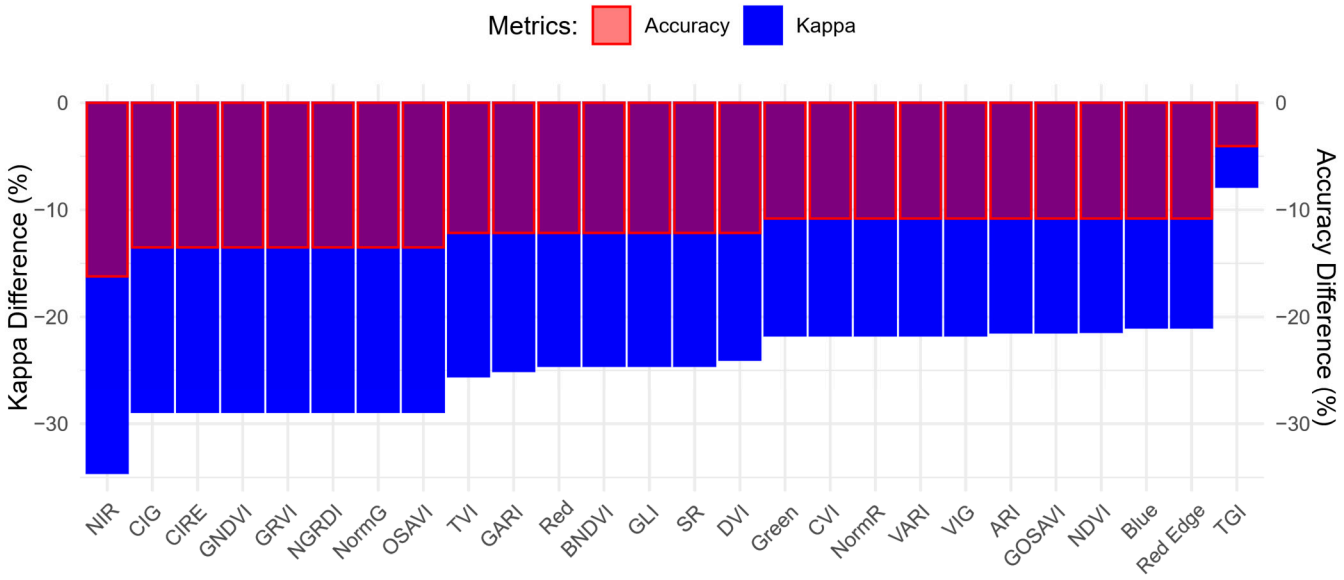


Figure 6. Differences in Kappa coefficient and accuracy for various vegetation indices. Red bars represent accuracy differences; blue bars indicate Kappa coefficient differences.

A direct visual comparison of the per-class confusion matrices for the baseline model (full feature set) and the B5-zeroed model is presented below (Figure 7). Of the 49 reference points labelled as mistletoe (class 1), 49 were correctly classified in the baseline model and 49 in the B5-zeroed model. Of the 5 reference points labelled as coniferous canopy (class 2), 5 were correctly classified in the baseline model and 5 in the B5-zeroed model. Of the 5 reference points labelled as deciduous canopy (class 3), 5 were correctly classified in the baseline model; in the B5-zeroed model, 4 were correctly classified, with 1 reference point classified as coniferous canopy (class 2). Of the 5 reference points labelled as dead trees (class 4), 4 were correctly classified in the baseline model and 1 in the B5-zeroed model, with 2 reference points classified as deciduous canopy (class 3) and 2 as ground and undergrowth (class 5). Of the 10 reference points labelled as ground and undergrowth (class 5), 9 were correctly classified in the baseline model and 3 in the B5-zeroed model, with 4 reference points classified as mistletoe (class 1) and 3 as deciduous canopy (class 3). Overall accuracy decreased from 0.97 to 0.84 between the baseline and the B5-zeroed model, and Cohen's Kappa from 0.95 to 0.61 (ΔKappa = −0.34).



Figure 7. Per-class confusion matrices illustrating the effect of zeroing the NIR (B5) band in the leave-one-out analysis of the spectral information potential assessment (Section 3.3). Left panel: baseline SVM trained on the full feature set (5 raw bands + 22 vegetation indices). Right panel: SVM trained with the B5 (NIR) feature column set to zero, with all remaining 26 features preserved. Both models were trained and evaluated on the 50/50 stratified hold-out split of the 190 training polygons (SVM with RBF kernel, C = 3, fixed random seed = 123). Row labels (Predicted) and column labels (Reference) refer to the five training classes: 1—mistletoe, 2—coniferous canopy, 3—deciduous canopy, 4—dead trees, 5—ground and undergrowth. Cell values are observation counts; cell colour intensity scales with the column-wise (per-reference-class) percentage.

3.4. Spectral Signatures of Vegetation Indices Across Classes

Expanding the information potential assessment (Sections 3.2 and 3.3), spectral signatures of the selected vegetation indices and raw bands are compared across three categories: non-infested crowns, infested crowns, and mistletoe polygons (class definitions in Section 2.4). Among RGB-based indices, NGRDI, VARI, VIG, and TGI exhibited strong differentiation of isolated mistletoe patches. These indices showed consistently higher mean values for mistletoe and minimal overlap with other classes. NDVI, TVI, and NormR also distinguished mistletoe from host crowns, though the magnitude of separation was less pronounced. NormG showed clearly elevated values for mistletoe, indicating higher discriminative capacity compared to other MS-based indices (Figure 8).

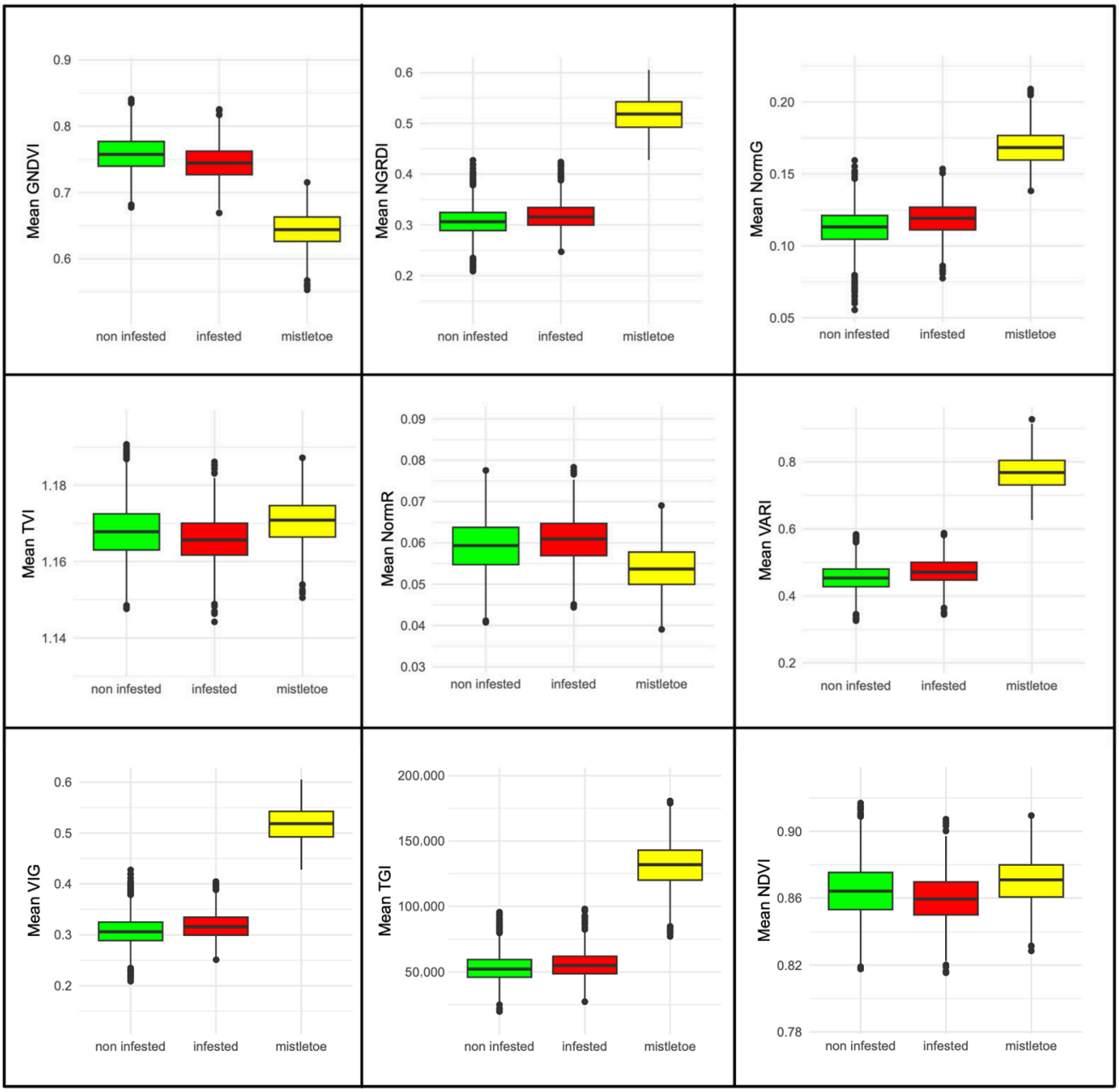


Figure 8. Mean values of selected vegetation indices for three categories: non-infested, infested, and mistletoe. Boxplots illustrate medians, interquartile ranges, whiskers (1.5 IQR), and outliers. Non-infested crowns (green), infested crowns (red), and mistletoe (yellow).

3.5. Raw Reflectance Analysis

In all five bands, the mean reflectance values for mistletoe were consistently higher than for the other two classes. The differences were particularly pronounced in the Red Edge (B4) and NIR (B5) bands. In RGB bands B2 (Green) and B3 (Red), mistletoe exhibited elevated reflectance with relatively clear separation from host crown categories. The Blue band (B1) displayed less pronounced separation, with overlapping distributions. The median value for mistletoe remained elevated across all bands (Figure 9).

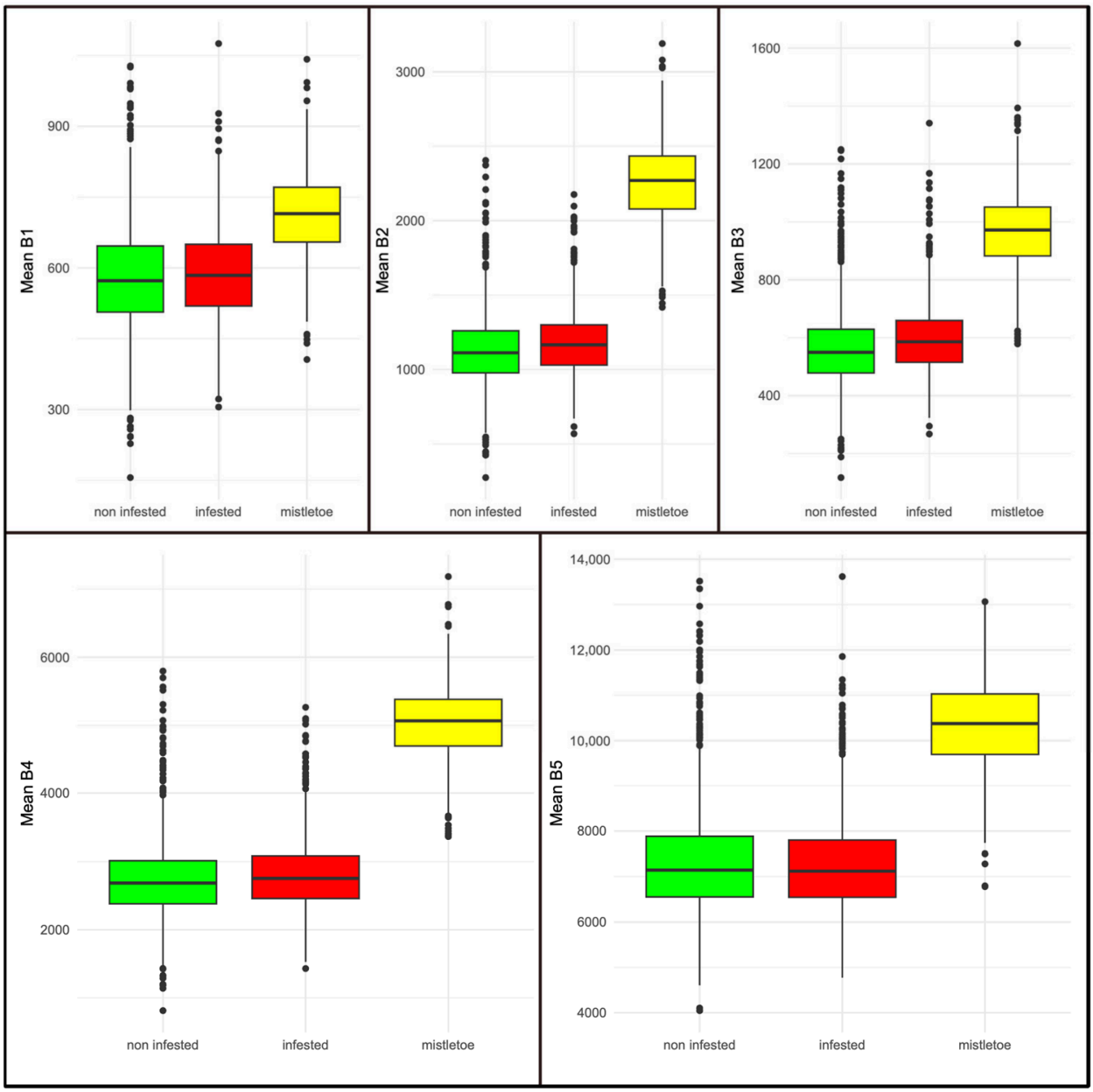


Figure 9. Distribution of mean reflectance values in spectral bands B1–B5 for three categories: non-infested crowns (green), infested crowns (red), and mistletoe (yellow).

3.6. Mistletoe Classification

The mistletoe classification in analyzed stand (22.5 ha) was performed in ArcGIS Pro using the segmentation parameters selected in Section 3.1, with the SVM classifier trained on the 190 training polygons using the five raw MicaSense multispectral bands (B1–B5) as input features (Section 2.5). The classification returned 1735 mistletoe biogroups with an average size of 0.28 m^2 and a total area of 489.11 m^2 (Figure 10). The smallest biogroup area was 0.02 m^2, while the largest was 2.87 m^2. Mistletoe infected 1710 of the 2917 detected trees (58.6%). The average number of biogroups per infected tree was approximately one (Figure 11). The Kappa coefficient was 0.74 and accuracy 0.82.

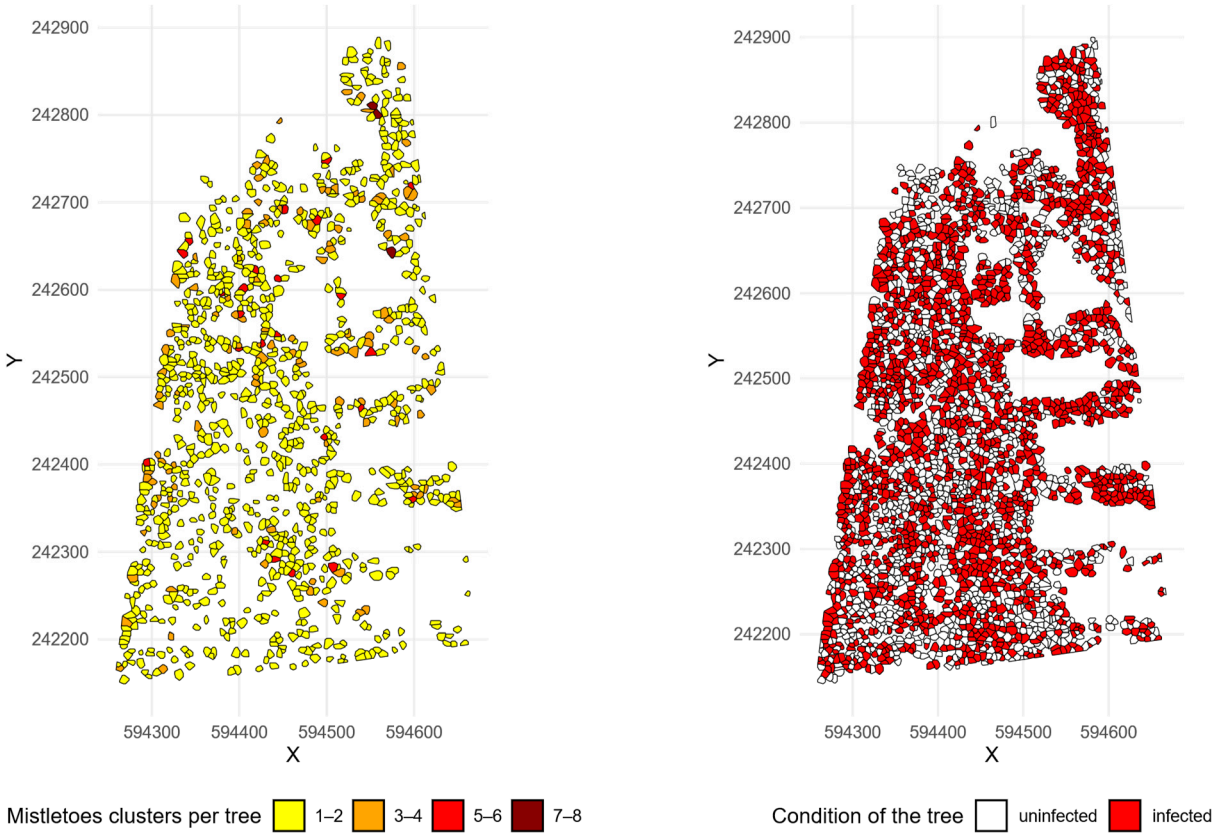


Figure 10. Classification results for compartment 83 (22.5 ha) showing detected mistletoe biogroups overlaid on the multispectral orthophoto.

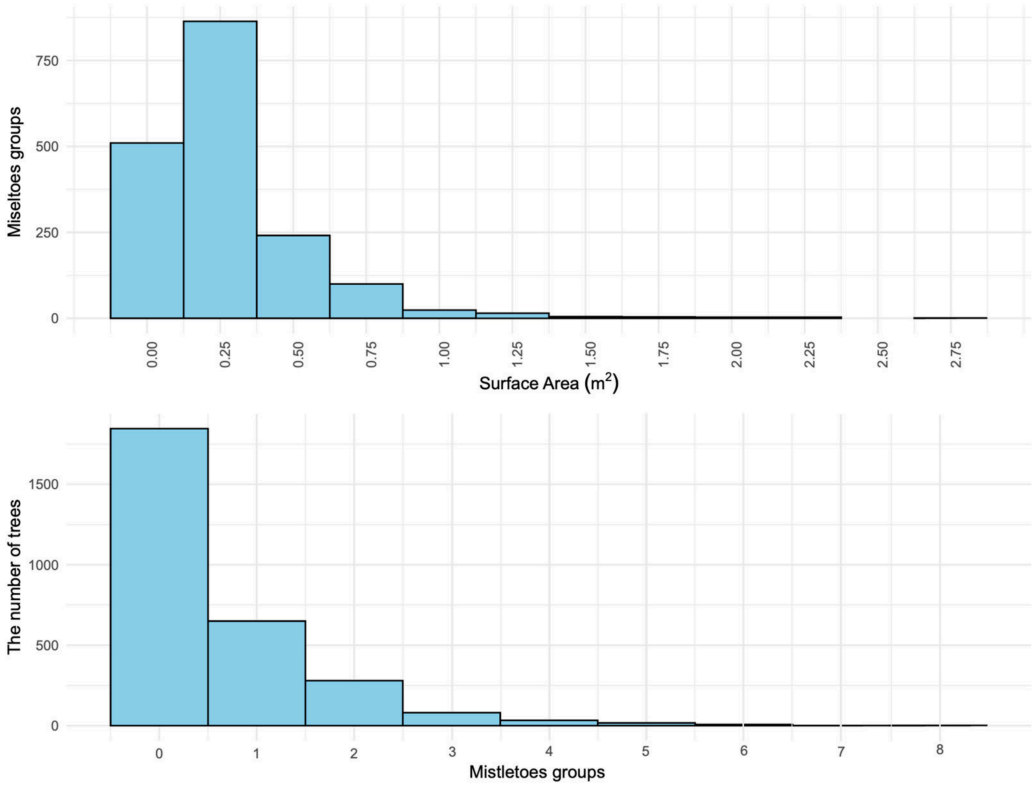


Figure 11. Top panel: Distribution of mistletoe biogroup surface area (m^2). Bottom panel: Number of trees in relation to the number of mistletoe biogroups per tree.

The map accuracy assessed against the 477 stratified random reference points (Section 2.7) yielded an overall accuracy of 0.82 and a Cohen's Kappa coefficient of 0.74. The per-class confusion matrix is presented below (Figure 12). Of the 48 reference points labelled as mistletoe (class 1), 40 were correctly classified by the model; 2 reference mistletoe points were classified as coniferous canopy (class 2), 3 as deciduous canopy (class 3), 2 as dead trees (class 4), and 1 as ground and undergrowth (class 5). Of the 247 reference points labelled as coniferous canopy (class 2), 238 were correctly classified, with the remaining 9 distributed across deciduous canopy (5), ground and undergrowth (3), and dead trees (1). Of the 71 reference points labelled as deciduous canopy (class 3), 43 were correctly classified, with the remaining 28 classified as coniferous canopy (14), ground and undergrowth (10), dead trees (3), and mistletoe (1). Of the 42 reference points labelled as dead trees (class 4), 30 were correctly classified, with the remaining 12 classified as mistletoe (3), deciduous canopy (5), and ground and undergrowth (4). Of the 69 reference points labelled as ground and undergrowth (class 5), 49 were correctly classified, with the remaining 20 classified as mistletoe (9), dead trees (5), deciduous canopy (4), and coniferous canopy (2).



Figure 12. Per-class confusion matrix for the mistletoe classification of the full 22.5-ha compartment, computed on 477 stratified random reference points generated on the classified raster using the Create Accuracy Assessment Points tool in ArcGIS Pro and manually labelled by the first author through visual photo-interpretation of the multispectral (NIR-Red-Green false-colour composite) and RGB orthomosaics (Section 2.7). Row labels (Predicted) refer to the SVM-classified class assigned to each reference point; column labels (Reference) refer to the operator-assigned reference class. Classes: 1—mistletoe, 2—coniferous canopy, 3—deciduous canopy, 4—dead trees, 5—ground and undergrowth. Cell values are observation counts; cell colour intensity scales with the column-wise (per-reference-class) percentage. Overall accuracy = 0.82, Cohen's Kappa = 0.74, n = 477.

4. Discussion

The occurrence of mistletoe in forests is a growing problem. The development of detection methods is an urgent need. Decreasing groundwater levels, drought stress, and climate change continue to create conditions conducive to mistletoe growth [11,12]. Dash et al. (2018) investigated whether multispectral data acquired from UAV platforms can monitor tree health and complement satellite data [17]. NDVI, RENDVI, and GNDVI indices were utilized to monitor physiological stress symptoms in pine stands growing in New Zealand (Pinus rigida D.Don). NDVI was identified as the most useful indicator for assessing stress-induced crown colour disturbance.

Maes et al. (2018) employed thermal infrared cameras to study mistletoe in eucalyptus trees in Australia [16]. Trees in their survey area were found to be infected at a rate of 68% [16]. Ančić et al. (2014) used hyperspectral imaging and the Spectral Angle Mapper (SAM) classifier over beech and fir stands in Croatia [18]. They concluded that detection of infection is possible and cost-effective, and recommended its use on a wider scale [18]. All the methods described above address only the detection of infection. The determination of the number of mistletoe biogroups and their areas has not been addressed.

In the current study, the use of high-resolution multispectral data from the Trinity F90+ UAV enabled the determination of 1710 infected trees out of 2917 detected trees. More than 1700 biogroups with a total area of almost 490 m^2 were identified. Four segmentation variants were tested. The variant based on a minimum segment size of 10 pixels produced the best compromise between biogroup count and area accuracy. Classifiers based on larger minimum segment sizes (20 pixels) detected fewer biogroups due to the fragmentation of mistletoe in middle crown parts. Single-pixel clustering overestimated the biogroup count due to isolated pixels and the splitting of biogroups.

The leave-one-out analysis identified NIR (B5) as the single most important spectral feature, followed by CIG, NormG, and GRVI among vegetation indices. The Blue band (B1) was the least informative. The high accuracy and Kappa values reported in this analysis (Kappa = 0.97; Sections 3.2 and 3.3) reflect the fact that the SVM classified pre-selected, manually verified training polygons that represent clean, characteristic examples of each class—not the full heterogeneous orthomosaic. As such, these values should be interpreted as a measure of the spectral discriminability of the feature set, rather than as the accuracy expected from operational classification of an entire scene; the latter is reported separately in Section 3.6 (Kappa = 0.74). Future work should expand the feature space to include higher-order segment statistics (minimum, maximum, standard deviation, coefficient of variation) and texture features (e.g., GLCM-derived metrics) to improve robustness to within-crown variability such as shadows and needle clumping.

The information potential assessment (Sections 3.2–3.5) and the mistletoe classification (Section 3.6) report two non-comparable Kappa values: the Kappa = 0.97 from the information potential assessment quantifies the spectral discriminability of the feature set on the 190 training polygons, while the Kappa = 0.74 from the mistletoe classification quantifies the accuracy of the classified map across the entire 22.5-ha compartment, validated against 477 spatially independent reference points. The two analyses are complementary but methodologically independent: the information potential assessment characterises which spectral features carry the most discriminative information, while the mistletoe classification produces the operational map.

The method described in this paper enables the determination of the number of biogroups per individual tree. A single infected tree in compartment 83 hosts approximately one cluster of mistletoe on average. The rapid development of artificial intelligence opens new possibilities for mistletoe detection. The method presented may serve as a starting

point for creating training datasets for neural networks. A neural network implemented in UAV onboard software could indicate mistletoe in real time during aerial surveys.

The choice of SVM as the classification algorithm in both the mistletoe classification (Section 2.5) and the spectral information potential assessment (Section 2.6) was based on its established performance for object-based classification of UAV multispectral imagery in forest environments [39,40], where SVM has been repeatedly reported to perform comparably to Random Forest and other ensemble classifiers when applied to high-dimensional spectral feature spaces with moderate training sample sizes. The objective of the present study was to characterise the discriminative information content of individual spectral features and to deliver a baseline mistletoe classification workflow, rather than to identify the optimal classifier or to optimise hyperparameters; a systematic multi-classifier benchmark including Random Forest and gradient boosting, applied to both analyses, is identified as a priority direction for future work (Section Limitations and Future Work).

Limitations and Future Work

The findings reported in this study should be interpreted in the context of several methodological constraints which are explicitly acknowledged here.

Spatial scope. All data originate from a single 22.5-ha forest compartment of mature Scots pine of comparable age, structure, and site conditions. The model was neither trained nor tested in stands with different densities, age classes, canopy closure levels, mixed-species compositions, diverse understory types, or contrasting soil and moisture regimes. The transferability of the proposed workflow to forests with more heterogeneous spectral backgrounds—for example mixed coniferous-deciduous stands, younger plantations, or sites with a more developed shrub layer—therefore remains to be tested. The present study should be regarded as an exploratory, proof-of-concept investigation aimed at establishing a baseline workflow and characterising the discriminative potential of UAV multispectral data for mistletoe detection in Scots pine. Multi-site validation across compartments and forest districts with contrasting stand characteristics is the principal direction of future work.

Temporal scope. The UAV campaign was conducted on a single date during the leaf-on growing season. Multi-temporal acquisitions spanning leaf-on and leaf-off conditions, as well as different times of day, may further enhance separability between mistletoe and host tree crowns and are identified as future work.

Feature space. The information potential assessment relied on segment-level mean reflectance and mean vegetation index values. Higher-order segment statistics (minimum, maximum, standard deviation, coefficient of variation) and texture features (e.g., GLCM-derived metrics) were not included in the feature space. Their inclusion could improve robustness to within-crown variability such as shadows and needle clumping, and is a natural direction for future work.

Classifier and hyperparameter selection. Both the mistletoe classification (Section 2.5) and the spectral information potential assessment (Section 2.6) were performed with SVM using default hyperparameters: the ArcGIS Pro Image Classification Wizard defaults for the operational map, and the kernlab defaults (RBF kernel, C = 3, automatic sigma estimation, no class weighting) for the information potential assessment. No formal grid-search hyperparameter tuning, sensitivity analysis, or comparison with alternative classifiers was performed in the present study. While SVM with default settings is a well-established choice for object-based classification of UAV multispectral imagery in forest environments (Section 4), a systematic multi-classifier benchmark—including Random Forest, gradient boosting, and ensemble methods—coupled with nested cross-validation hyperparame-

ter tuning, applied separately to both analyses, is identified as a priority direction for future work.

Per-class sample sizes. For the spectral information potential assessment, the training set comprised 100 mistletoe polygons and 90 non-mistletoe polygons distributed across four background classes (20 polygons each for coniferous canopy, deciduous canopy, dead trees; 30 for ground and undergrowth). Within a single uniform compartment, this number of operator-verified polygons is sufficient to capture the within-class spectral variability of each background class; however, expanding the training set across multiple compartments would strengthen the generalisability of the discriminative findings.

Tree detection accuracy. The ALS-based tree detection pipeline used standard parameters from the lidR package (Section 2.4); however, the accuracy of the detected tree count (2917 trees in the 22.5-ha compartment) was not formally validated against an independent manual count. The 58.6% infection rate and the 1735 biogroups reported in Section 3.6 are therefore derived from the detected tree set and inherit any over- or under-detection of the lidR pipeline. Formal validation of tree detection accuracy is identified as future work.

Confidence intervals. Confidence intervals on the inventory outputs (infection rate, total biogroup count, total biogroup area) and on the per-class accuracy metrics were not computed in the present study, given its exploratory scope and the focus on establishing the methodological workflow. The reported figures should be regarded as point estimates from the present compartment. Bootstrap confidence intervals computed over the 477 stratified random reference points (Section 2.7) are identified as a methodological refinement for follow-up studies on multiple compartments.

5. Conclusions

In the current study, the potential of UAV-based multispectral and RGB imagery for detecting common mistletoe (*Viscum album* ssp. *austriacum*) in Scots pine stands was investigated. The study was conducted in the Niepołomice Primeval Forest using a fixed-wing Trinity F90+ UAV equipped with a MicaSense RedEdge-M multispectral camera and a Sony UMC-R10C RGB camera. Twenty-two vegetation indices were calculated and evaluated for their information potential using SVM classification.

The highest classification performance was achieved by combining NIR and Red Edge bands with vegetation indices, reaching an accuracy of 0.99 and a Kappa coefficient of 0.97. NormG and CIG demonstrated the greatest discriminative capacity for mistletoe detection. The NIR band (B5) was identified as the single most important variable, with its removal causing a Kappa decrease exceeding 30%. The full-area classification of compartment 83 (22.5 ha) revealed that 58.6% of all detected trees were infected, comprising 1735 biogroups with a total area of 489 m^2 and a Kappa coefficient of 0.74.

Based on the results, UAV-based multispectral data combined with green-sensitive and NIR-based vegetation indices enable effective non-invasive monitoring of mistletoe infestation at the individual tree level. A camera system with at least NIR, Red, and Green channels is recommended for operational mistletoe detection. Future research should focus on higher-resolution cameras, thermal infrared sensors, oblique imagery, and high-density UAV Laser Scanning (ULS). The integration of these technologies with deep learning approaches may represent the most effective method for large-scale operational monitoring of mistletoe occurrence.

Author Contributions: Conceptualization, J.M. and P.W.; methodology, J.M. and P.W.; software, J.M.; validation, J.M., formal analysis, J.M.; investigation, J.M.; resources, J.M. and P.W.; data curation, J.M.; writing—original draft preparation, J.M., L.T.-C., J.S., M.S. and P.W.; writing—review and editing, J.M., L.T.-C., J.S. and M.S.; visualization, J.M.; supervision, J.M. and P.W.; project administration, J.M. All authors have read and agreed to the published version of the manuscript.

Funding: This research received no external funding.

Data Availability Statement: The ALS LiDAR data were obtained from the GUGiK repository. Forest digital map data were sourced from the Forest Data Bank (www.bdl.lasy.gov.pl/portal/; accessed on 21 January 2022). UAV imagery data are available from the corresponding author upon reasonable request.

Acknowledgments: The authors express gratitude to Piotr Weżyk for supervising the engineering thesis which formed the basis for this article. Appreciation is extended to Luiza Tymińska-Czabańska and Paweł Hawryło for their constructive criticism and invaluable advice. The authors also thank ProGea SKY Ltd. for providing data free of charge.

Conflicts of Interest: Author Piotr Wężyk was employed by the company ProGea SKY Ltd. The remaining authors declare that the research was conducted in the absence of any commercial or financial relationships that could be construed as a potential conflict of interest.

Abbreviations

The following abbreviations are used in this manuscript:

ALS	Airborne Laser Scanning
CHM	Canopy Height Model
DSM	Digital Surface Model
GNSS	Global Navigation Satellite System
GSD	Ground Sampling Distance
MS	Multispectral
NIR	Near-Infrared
PPK	Post-Processing Kinematic
RGB	Red, Green, Blue
SVM	Support Vector Machine
UAV	Unmanned Aerial Vehicle
ULS	UAV Laser Scanning
VI	Vegetation Index
VLOS	Visual Line of Sight
VTOL	Vertical Take-Off and Landing

References

1. Bernier, P.; Schoene, D. Adapting Forests and Their Management to Climate Change: An Overview. *Unasylva* **2009**, *60*, 5–11.
2. Jamali, S.; Olsson, P.-O.; Ghorbanian, A.; Müller, M. Examining the Potential for Early Detection of Spruce Bark Beetle Attacks Using Multi-Temporal Sentinel-2 and Harvester Data. *ISPRS J. Photogramm. Remote Sens.* **2023**, *205*, 352–366. [CrossRef]
3. Sangüesa-Barreda, G.; Linares, J.C.; Julio Camarero, J. Drought and Mistletoe Reduce Growth and Water-Use Efficiency of Scots Pine. *For. Ecol. Manag.* **2013**, *296*, 64–73. [CrossRef]
4. Turner, R.J.; Smith, P. Mistletoes Increasing in Eucalypt Forest near Eden, New South Wales. *Aust. J. Bot.* **2016**, *64*, 171–179. [CrossRef]
5. Senf, C.; Seidl, R. Persistent Impacts of the 2018 Drought on Forest Disturbance Regimes in Europe. *Biogeosciences* **2021**, *18*, 5223–5230. [CrossRef]
6. Iszkuło, G.; Armatys, L.; Dering, M.; Ksepko, M.; Tomaszewski, D.; Ważna, A.; Giertych, M.J. Mistletoe as a Threat to the Health State of Coniferous Forest. *Sylwan* **2020**, *164*, 226–236.
7. Państwowe Gospodarstwo Leśne Lasy Państwowe. *Raport o Stanie Lasów w Polsce 2022*; State Forests: Warszawa, Poland, 2023.
8. Walas, Ł.; Kędziora, W.; Ksepko, M.; Rabska, M.; Tomaszewski, D.; Thomas, P.A.; Wójcik, R.; Iszkuło, G. The Future of *Viscum album* L. in Europe Will Be Shaped by Temperature and Host Availability. *Sci. Rep.* **2022**, *12*, 16741. [CrossRef]
9. Schaffer, B. Effects of Comandra Blister Rust and Dwarf Mistletoe on Cone and Seed Production of Lodgepole Pine. *Plant Dis.* **1983**, *67*, 215–217. [CrossRef]
10. Jasiczek, N.; Giertych, M.J.; Suszka, J. Influence of Mistletoe (*Viscum album*) on the Quality of Scots Pine (*Pinus sylvestris*) Seeds. *Sylwan* **2017**, *161*, 558–564.
11. Sangüesa-Barreda, G.; Linares, J.C.; Camarero, J.J. Mistletoe effects on Scots pine decline following drought events: Insights from within-tree spatial patterns, growth and carbohydrates. *Tree Physiol.* **2012**, *32*, 585–598. [CrossRef] [PubMed]

12. Pilichowski, S.; Filip, R.; Kościelska, A.; Zaroffe, G.; Żyźniewska, A.; Iszkuło, G. Wpływ *Viscum album* ssp. *austriacum* (Wiesb.) Vollm. Na Przyrost Radialny *Pinus sylvestris* L. *Sylwan* **2018**, *162*, 452–459.
13. Shaw, D.C.; Chen, J.; Freeman, E.A.; Braun, D.M. Spatial and Population Characteristics of Dwarf Mistletoe Infected Trees in an Old-Growth Douglas-Fir—Western Hemlock Forest. *Can. J. For. Res.* **2005**, *35*, 990–1001. [CrossRef]
14. Kędziora, W.; Bobińska, A.; Wójcik, R. Proposition of a Large-Scale Mistletoe Inventory Method. *Sylwan* **2020**, *164*, 568–575.
15. Piętka, J.; Małecki, M.; Niewiński, K.; Kędziora, W. How Wrong Are We in Estimating the Abundance of Mistletoe Occurring on Scots Pine?—A Case Study from Central Europe. *Balt. For.* **2023**, *29*, 717. [CrossRef]
16. Maes, W.H.; Huete, A.R.; Avino, M.; Boer, M.M.; Dehaan, R.; Pendall, E.; Griebel, A.; Steppe, K. Can UAV-Based Infrared Thermography Be Used to Study Plant-Parasite Interactions between Mistletoe and Eucalypt Trees? *Remote Sens.* **2018**, *10*, 2062. [CrossRef]
17. Dash, J.P.; Pearse, G.D.; Watt, M.S. UAV Multispectral Imagery Can Complement Satellite Data for Monitoring Forest Health. *Remote Sens.* **2018**, *10*, 1216. [CrossRef]
18. Ančić, M.; Pernar, R.; Bajić, M.; Seletković, A.; Kolić, J. Detecting Mistletoe Infestation on Silver Fir Using Hyperspectral Images. *iForest* **2014**, *7*, 85–89. [CrossRef]
19. Roussel, J.R.; Auty, D. *lidR: Airborne LiDAR Data Manipulation and Visualization for Forestry Applications*; R CRAN Proj.; R Project: Vienna, Austria, 2018; Volume 1.
20. Hijmans, R.J. *Raster: Geographic Analysis and Modeling with Raster Data*, Version 3.1-5. R Package. R Project: Vienna, Austria, 2020.
21. Montero, D.; Aybar, C.; Mahecha, M.D.; Martinuzzi, F.; Söchting, M.; Wieneke, S. A Standardized Catalogue of Spectral Indices to Advance the Use of Remote Sensing in Earth System Research. *Sci. Data* **2023**, *10*, 197. [CrossRef] [PubMed]
22. Louhaichi, M.; Borman, M.M.; Johnson, D.E. Spatially Located Platform and Aerial Photography for Documentation of Grazing Impacts on Wheat. *Geocarto Int.* **2001**, *16*, 65–70. [CrossRef]
23. Tucker, C.J. Red and Photographic Infrared Linear Combinations for Monitoring Vegetation. *Remote Sens. Environ.* **1979**, *8*, 127–150. [CrossRef]
24. Hunt, E.R.; Doraiswamy, P.C.; McMurtrey, J.E.; Daughtry, C.S.T.; Perry, E.M.; Akhmedov, B. A Visible Band Index for Remote Sensing Leaf Chlorophyll Content at the Canopy Scale. *Int. J. Appl. Earth Obs. Geoinf.* **2013**, *21*, 103–112. [CrossRef]
25. Gitelson, A.A.; Kaufman, Y.J.; Stark, R.; Rundquist, D. Novel Algorithms for Remote Estimation of Vegetation Fraction. *Remote Sens. Environ.* **2002**, *80*, 76–87. [CrossRef]
26. Gitelson, A.A.; Merzlyak, M.N.; Chivkunova, O.B. Optical Properties and Nondestructive Estimation of Anthocyanin Content in Plant Leaves. *Photochem. Photobiol.* **2001**, *74*, 38–45. [CrossRef]
27. Wang, F.; Huang, J.; Tang, Y.; Wang, X. New Vegetation Index and Its Application in Estimating Leaf Area Index of Rice. *Rice Sci.* **2007**, *14*, 195–203. [CrossRef]
28. Gitelson, A.A.; Gritz, Y.; Merzlyak, M.N. Relationships between Leaf Chlorophyll Content and Spectral Reflectance and Algorithms for Non-Destructive Chlorophyll Assessment in Higher Plant Leaves. *J. Plant Physiol.* **2003**, *160*, 271–282. [CrossRef]
29. Vincini, M.; Frazzi, E. Comparing Narrow and Broad-Band Vegetation Indices to Estimate Leaf Chlorophyll Content in Planophile Crop Canopies. *Precis. Agric.* **2011**, *12*, 334–344. [CrossRef]
30. Roujean, J.-L.; Bréon, F.-M. Estimating PAR Absorbed by Vegetation from Bidirectional Reflectance Measurements. *Remote Sens. Environ.* **1995**, *51*, 375–384. [CrossRef]
31. Gitelson, A.A.; Kaufman, Y.J.; Merzlyak, M.N. Use of a Green Channel in Remote Sensing of Global Vegetation from EOS-MODIS. *Remote Sens. Environ.* **1996**, *58*, 289–298. [CrossRef]
32. Sripada, R.P.; Heiniger, R.W.; White, J.G.; Weisz, R. Aerial Color Infrared Photography for Determining Late-Season Nitrogen Requirements in Corn. *Agron. J.* **2005**, *97*, 1443–1451. [CrossRef]
33. Rouse, J.W., Jr.; Haas, R.H.; Schell, J.A.; Deering, D.W. Monitoring Vegetation Systems in the Great Plains with ERTS. In Proceedings of the Third ERTS-1 Symposium, Washington, DC, USA, 10–14 December 1973; pp. 309–317.
34. Marcial-Pablo, M.J.; Gonzalez-Sanchez, A.; Jimenez-Jimenez, S.I.; Ontiveros-Capurata, R.E.; Ojeda-Bustamante, W. Estimation of vegetation fraction using RGB and multispectral images from UAV. *Int. J. Remote Sens.* **2018**, *40*, 420–438. [CrossRef]
35. Rondeaux, G.; Steven, M.; Baret, F. Optimization of Soil-Adjusted Vegetation Indices. *Remote Sens. Environ.* **1996**, *55*, 95–107. [CrossRef]
36. Jordan, C.F. Derivation of Leaf-Area Index from Quality of Light on the Forest Floor. *Ecology* **1969**, *50*, 663–666. [CrossRef]
37. Roussel, J.; Auty, D.; Coops, N.C.; Tompalski, P.; Goodbody, T.R.H.; Sánchez, A.; Bourdon, J.; De Boissieu, F.; Achim, A. lidR: An R Package for Analysis of Airborne Laser Scanning (ALS) Data. *Remote Sens. Environ.* **2020**, *251*, 112061. [CrossRef]
38. Karatzoglou, A.; Hornik, K.; Smola, A.; Zeileis, A. kernlab—An S4 Package for Kernel Methods in R. *J. Stat. Softw.* **2004**, *11*, 1–20. [CrossRef]

39. Sothe, C.; Almeida, C.M.; Liesenberg, V.; Schimalski, M.B. Evaluating Sentinel-2 and Landsat-8 Data to Map Sucessional Forest Stages in a Subtropical Forest in Southern Brazil. *Remote Sens.* **2017**, *9*, 838. [CrossRef]
40. Maxwell, A.E.; Warner, T.A.; Fang, F. Implementation of Machine-Learning Classification in Remote Sensing: An Applied Review. *Int. J. Remote Sens.* **2018**, *39*, 2784–2817. [CrossRef]

Disclaimer/Publisher's Note: The statements, opinions and data contained in all publications are solely those of the individual author(s) and contributor(s) and not of MDPI and/or the editor(s). MDPI and/or the editor(s) disclaim responsibility for any injury to people or property resulting from any ideas, methods, instructions or products referred to in the content.